The Egyptian Journal of Remote Sensing and Space Sciences (2014) 17, 17–27

National Authority for Remote Sensing and Space Sciences

The Egyptian Journal of Remote Sensing and Space Sciences

www.elsevier.com/locate/ejrs
www.sciencedirect.com

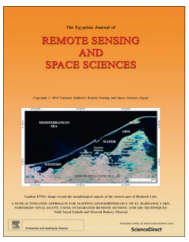

RESEARCH PAPER

Enhanced sharpening procedures on edge difference and water stress index basis over heterogeneous landscape of sub-humid region

Martin I. Bayala [a,b,*], Raúl E. Rivas [a,b]

[a] Instituto de Hidrologa de Llanuras "Dr. Eduardo J. Usunoff", Pje. Arroyo Seco S/N, 7000 Tandil, Argentina
[b] Comisión de Investigaciones Científicas de la provincia de Buenos Aires, Argentina

Received 11 February 2014; revised 8 May 2014; accepted 17 May 2014
Available online 2 July 2014

KEYWORDS

EOS-MODIS;
Landsat TM;
Land Surface Temperature (LST);
Sharpening models;
Data validation

Abstract Land Surface Temperature (LST) is a key parameter in the energy balance model. However, the spatial resolution of the retrieved LST from sensors with high temporal resolution is not accurate enough to be used in local-scale studies. To explore the LST–Normalised Difference Vegetation Index relationship potential and obtain thermal images with high spatial resolution, six enhanced image sharpening techniques were assessed: the disaggregation procedure for radiometric surface temperatures (T_sHARP), the Dry Edge Quadratic Function, the Difference of Edges (T_s^*DL) and three models supported by the relationship of surface temperature and water stress of vegetation (Normalised Difference Water Index, Normalised Difference Infrared Index and Soil wetness index). Energy Balance Station data and *in situ* measurements were used to validate the enhanced LST images over a mixed agricultural landscape in the sub-humid Pampean Region of Argentina (PRA), during 2006–2010. Landsat Thematic Mapper (TM) and Moderate Resolution Imaging Spectroradiometer (EOS-MODIS) thermal datasets were assessed for different spatial resolutions (e.g., 960, 720 and 240 m) and the performances were compared with global and local T_sHARP procedures. Results suggest that the T_s^*DL technique is the most adequate for simulating LST to high spatial resolution over the heterogeneous landscape of a sub-humid region, showing an average root mean square error of less than 1 K.

* Corresponding author at: Instituto de Hidrología de Llanuras "Dr. Eduardo J. Usunoff", Pje. Arroyo Seco S/N, 7000 Tandil, Argentina. Tel.: +54 2494439520.
E-mail address: martin.bayala@rec.unicen.edu.ar (M.I. Bayala).
Peer review under responsibility of National Authority for Remote Sensing and Space Sciences.

ELSEVIER Production and hosting by Elsevier

1. Introduction

Land Surface Temperature (LST) products with moderate and high spatial and temporal resolutions are needed for many applications in environmental monitoring and emergency early warning response. Improvements in the spatial resolution of LST images could extend their potential significantly (Yang et al., 2011). Thus, efforts have been made to obtain a correct

1110-9823 © 2014 Production and hosting by Elsevier B.V. on behalf of National Authority for Remote Sensing and Space Sciences.
http://dx.doi.org/10.1016/j.ejrs.2014.05.002

estimation of Land Surface Temperature (LST) by downscaling resolution over the PRA. However, owing to the relatively lower thermal radiation that is emitted by land surfaces in such areas, most satellite sensors are incapable of providing as much fine-scale information in the TIR wavelengths compared with the visible/near infrared (VNIR) and short wave infrared (SWIR). Currently, various types of sensors operate on-board satellite platforms with bands in the VIS–SWIR (0.4–7.3 μm) and TIR (8.0–14.0 μm) spectral ranges attuned to different spatial resolutions. Sensors such as EOS-MODIS provide TIR bands with coarse spatial resolutions ($\geqslant$1 km) and VNIR bands with moderate spatial resolution (250 m) with a fine temporal resolution ($\leqslant$1 day). Sensors with moderate spatial resolution thermal data (>250 m) such as the Advanced Spaceborne Thermal Emission Reflection Radiometer (ASTER), Enhanced Thematic Mapper Plus (ETM+) and Landsat Data Continuity Mission (LDCM) are available with a coarse temporal resolution (16 days or request).

The concept of sharpening refers to disaggregating an image with coarse spatial resolution to a downscaling of the spatial resolution, by combining two or more image sets from the same or different sensors, preserving the radiometric content of the image. The sharpening procedure must ensure an accurate spatial description of the LST variability and preserve the coherence in the radiometry of the original TIR band (Rodriguez-Galiano et al., 2012). Different sharpening methods for enhancing the spatial resolution of LST have been developed, such as fractal interpolation (Kim and Barrows, 2002), empirical relationships (Kustas et al., 2003; Agam et al., 2007a; Jeganathan et al., 2011), analytical and physical models (Merlin et al., 2008), linear or spectral mixture models (Liu and Pu, 2008; Zurita-Milla et al., 2009), sequential disaggregation (Merlin et al., 2009) and geostatistical downscaling cokriging (Rodriguez-Galiano et al., 2012).

The Disaggregation procedure for Radiometric Surface Temperature technique (*DisTrad*) was proposed by Kustas et al. (2003), using the empirical relationship between LST and the Normalised Difference Vegetation Index (NDVI) (Rouse et al., 1974). Agam et al. (2007a,b) redefined the *DisTrad* procedure under the assumption that the LST variability is controlled by the fraction vegetation cover (f_c) and called it T_sHARP. The *DisTrad* technique disaggregates a coarse spatial resolution LST image to fine spatial resolution. It is defined by the negative slope variation generated in a least squares regression model fitted to the relation between the LST and NDVI, where both are from a coarse spatial resolution image (denoted by the subscript *LR*) (Kustas et al., 2003; Jeganathan et al., 2011; Yang et al., 2011). The sharpening methodology is as follows:

$$LST^{*}(NDVI_{LR}) = f(NDVI_{LR}) \quad (1)$$

The slope and intercept parameters of the least squares regression model are applied to the coarse spatial resolution NDVI image to simulate a coarse spatial resolution thermal image (the star symbol indicates a predicted LST value). The residual error (Δt_{LR}) is due to forces driving surface temperature other than the amount of vegetation cover (e.g., soil moisture) (Kustas et al., 2003; Agam et al., 2007a) (see Fig. 1). The residual error can be assessed at the coarse scale as follows:

$$\Delta t_{LR} = LST_{LR} - LST^{*}_{LR} \quad (2)$$

Therefore, the sharpened sub-pixel temperatures within each coarse pixel are computed by Eq. (3), using the estimated coefficients derived from the coarse spatial resolution data on the NDVI to the high spatial resolution (denoted by the subscript HR) (Agam et al., 2007a).

$$LST^{*}_{HR} = LST^{*}(NDVI_{HR}) + \Delta t_{LR} \quad (3)$$

Here, Δt_{LR} is the coarse spatial resolution residual added to the fine spatial resolution predicted temperature to increase the accuracy of the simulated image, considering the proportion of water in the plant-soil system. This procedure requires that a range of surface temperature and vegetation indices be present within the image scene, in order to develop a significant regression relationship. Therefore, *DisTrad* does not perform well over scenes in which there is little variability in surface temperature (e.g., night-time and early morning). Furthermore, the water body and cloud pixels were not considered when fitting the regression model because these tend to be outliers in the NDVI-LST relationship (Agam et al., 2007a).

The inverse linear relationship established widely between vegetation cover and LST is used for enhanced sharpening procedures. This relationship is controlled by various factors including the thermal properties of the surface, soil and vegetation water content, evapotranspiration and net radiation (Sandholt et al., 2002; Holzman et al., 2014). Also, it is influenced strongly by annual seasonality. Sun and Kufatos (2007) observed that the relationship is negative in warm seasons and positive in the winter. Hence, the current study assumes a negative relationship due to the warm climatic conditions over the PRA.

Many studies on sharpening have focused on the statistical regression methods taking into account the NDVI-LST relationship (Kustas et al., 2004; Li et al., 2008; Merlin et al., 2009; Yang et al., 2011). However, there are few background studies on the above sharpening techniques based on the use of the integrated dry and wet edge. Chen et al. (2010) used the dry and wet edge to develop a model called Soil Wetness Index Stepwise Fitting (SWISF) based on the Soil Wetness Index (SWI).

The aim of this paper is to research the application and evaluate the results of six different enhanced sharpening thermal models based on the NDVI-LST relationship and to determine the most accurate technique with ground-based radiative temperature (T_{rad}) measurements over the heterogeneous landscape of the Pampean Region of Argentina.

2. Methodology

2.1. Enhanced sharpening basis functions

Mixed vegetation cover is a typical feature of the land cover of the PRA. This heterogeneous area is covered with a mixture of crops, bare soil, water and small-scale impervious components (see Section 3). To obtain high-temporal resolution temperatures of individual agricultural fields to support drought monitoring and energy balance studies, six different sharpening methodologies based on the T_sHARP technique were employed with the aim of improving sub-pixel LST estimations. The first model uses the fitted dry edge extracted from the 2nd-degree polynomial regression between the LST and NDVI relationship, which is called the Dry Edge Quadratic

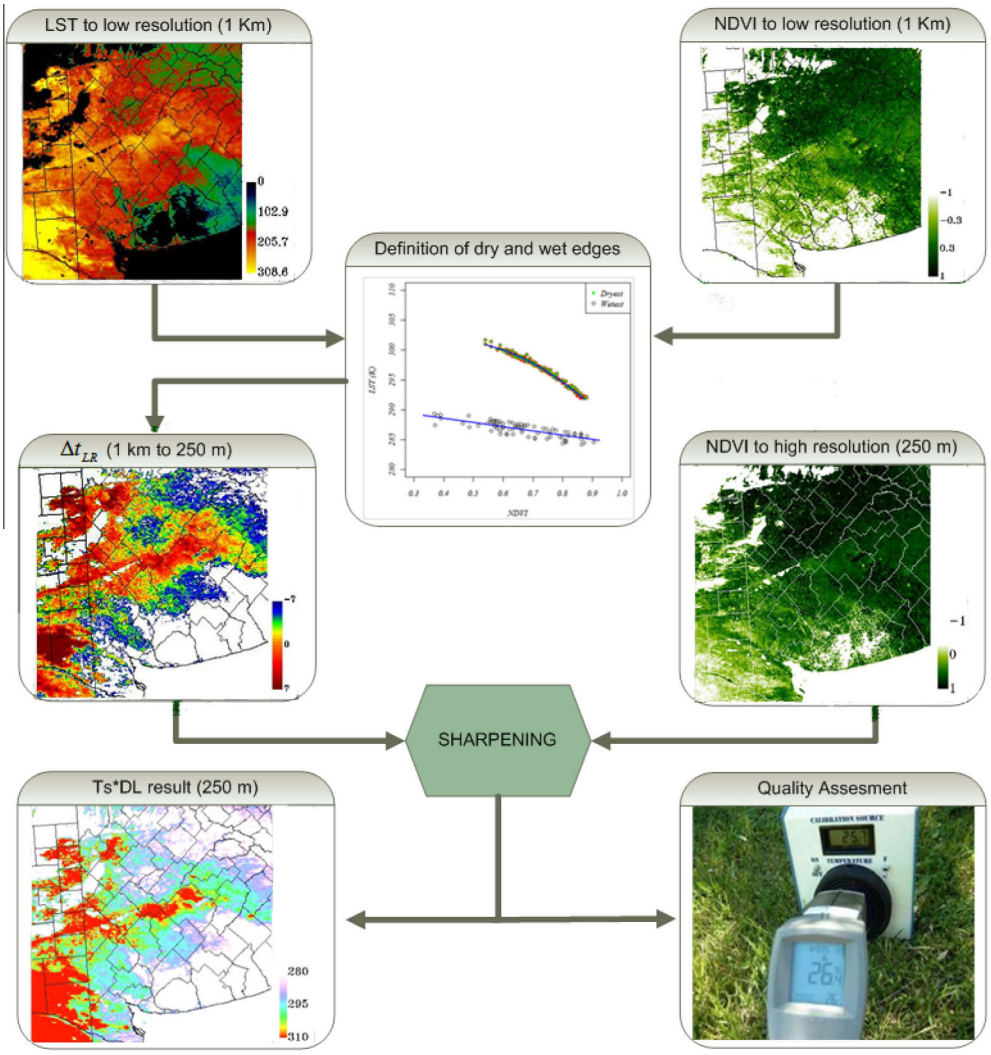

Figure 1 Flowchart of the T_s^*DL methodology.

Function (*FCLS*) (Fig. 1, *Definition of Dry and Wet edges*). The simulated LST image to high resolution can be expressed as:

$$T_s^*FCLS = a(NDVI_{HR})^2 + b(NDVI_{HR}) + c + \Delta t \quad (4)$$

Here, Δt_{LR} is presented in Eq. (2) and a, b and c are scene-specific parameters derived from the regression analysis.

For the last two decades, some authors (Kustas et al., 2003; Chen et al., 2010 and Chen et al., 2014) have compared the linear and quadratic fitting in different landscapes, dataset and spatial resolutions. The statistic results have shown that the quadratic fitting is better than the linear regression for agricultural (Kustas et al., 2003) and urban areas (Chen et al., 2014). Therefore, a physical basis over quadratic dry edge fitting was assumed, as the LST shows the maximum value (vertex of the function) when the coverage of vegetation is negligible (NDVI approaches zero). This resampling technique considers the major factors of different land cover types that impact the thermal properties of pixels within mixed land cover types.

To improve the T_s^*FCLS technique, the T_s^*DL model was developed using an estimation of moisture difference based on the subtraction between the wet and dry edge, which is expressed as:

$$T_s^*DL = T_s^*FCLS_{HR} + \Delta L \quad (5)$$

$T_s^*FCLS_{HR}$ is the estimated high resolution temperature image from Eq. (4) and ΔL is the subtraction between the wet (T_s^*FLLH) and dry edge (T_s^*FCLS) simulated high resolution temperature image. Fig. 1 shows the general procedure of the T_S^*DL model for obtaining LST images with enhanced spatial resolution simulated over the EOS-MODIS scene acquired on 23 February 2010.

A characteristic of the T_sHARP method is that it does not take into account that for a determinate NDVI value as there may be two different LST values. To address this issue, we needed to increase the thermal variability of the image simulated from the Stress Water Indices (SWIs). Fig. 2 shows the LST, NDVI and NDWI relationship, which may indicate a high dispersion of NDWI values with respect to LST values; the NDVI indicates a narrow range of values (0.82 ± 0.2) instead.

Based on the above inference, a refined rectification approach from adequate soil moisture estimations, using stress hydric indices, was proposed:

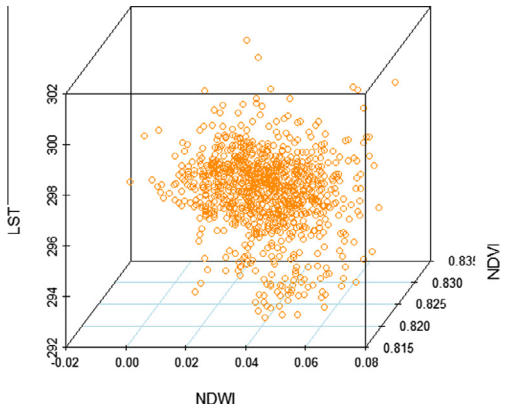

Figure 2 Example of 3-D scatter plot between the LST, NDVI and NWDI relationship.

$$T_s^* NDWI = T_s^* DL_{HR} * \left(\frac{NDWI - NDWI_{\min}}{NDWI_{\max} - NDWI_{\min}} \right)_{HR} \quad (6)$$

$$T_s^* NDII = T_s^* DL_{HR} * \left(\frac{NDII - NDII_{\min}}{NDII_{\max} - NDII_{\min}} \right)_{HR} \quad (7)$$

$$T_s^* SWI = T_s^* DL_{HR} * \left(\frac{LST_{\max} - LST}{LST_{\max} - LST_{\min}} \right)_{HR} \quad (8)$$

where NDWI is the Normalised Difference Water Index proposed by Gao (1996), NDII is the Normalised Difference Infrared Index proposed by Hardisky et al. (1983) and Soil Water Index (SWI) proposed by Mallick et al. (2009). The monitoring of the water content of the soil and vegetation (g H_2O m^{-2}) was performed using the absorption properties of vegetation water in the NIR band and sensitivity characteristics of water absorption difference in the SWIR band. The NDWI uses the spectral interval between 0.9 μm (NIR) and 1.2 μm (SWIR), whereas the NDII is based on the 0.9–1.6 μm interval. It should be noted that some sharpening procedures are limited in their application to some sensors owing to the unavailability of bands in the VNIR range.

3. Study area

The study region is located in Tandil, Buenos Aires province, on the PRA (Fig. 3). It is within a sub-humid temperate climate with a few hydric deficits and a mean air temperature of 14 °C, reaching a mean maximum summer air temperature of 295.1 K and a mean minimum winter air temperature of 280.1 K. The mean relative humidity of the air is 70%, the average wind speed is 3 m s^{-1} and the mean sun radiation received is 186 Wm^{-2} (Carmona et al., 2012).

From the perspective of land use, the selected area is characterised by the presence of heterogenic crops, from the 1st and 2nd soybean to bare soil. Agriculture is the main land use, although there are isolated urban uses and unproductive areas characterised by the presence of the *orographic system of Tandilia*.

4. Experimental setup

Two discontinuous pairs of images corresponding to the Landsat 5 Thematic Mapper and EOS-MODIS satellite sensors with the same path and row (225/86) were acquired on 10 November 2006 and 23 February 2010, for the ground validation dataset. Landsat 5 TM images with a spatial resolution of 30 m in the VNIR and 120 m in the thermal region with a revisit period of 16 days were utilised as reference data for model building as moderate-high resolution images. EOS-MODIS images with a spatial resolution of 250 and 500 m in the VNIR spectral region and 1000 m in the thermal region were procured because of their low spatial resolution and high revisit frequency (1 day).

The calibrated radiance of thermal, visible and NIR bands at 1 km, 500 m and 250 m (MOD021 km, MOD02HKM and MOD02QKM) and column water vapour (MOD05) products were used to retrieve the LST and vegetation index images. The EOS-MODIS dataset was matched spatially with the reference Landsat data through common ground control points to reduce prediction errors due to spatial mismatch.

The quality-sharpened image was assessed in terms of the true ground and image data. The validation procedure was carried out using a ground T_R dataset measured by a high precision IRR-1505 sensor (Apogee Instruments, Inc.) with an estimation error of ±0.2 K between 258.1 and 333.1 K, spectral interval between 8 and 14 μm and IFOV angle of 22°. The IRR-1505 sensor integrates the Energy Balance Station (EBS) data, located over a soybean field at Laura Laufú farm (37° 14′S 59° 34′W) (Fig. 3). A dataset of 38 *in situ* measurements over wheat crops (37°06′45″S; 58°58′50″W) was acquired with an Everest IRT radiometer (Everest Interscience Inc.), which measures temperatures from 233.1 K to 373.1 K with ±0.3 K accuracy from 273.1 K to 323.1 K. The calibration of radiometers was performed using a reference black body (Everest Model 1000), making measurements before, during and after the completion of the transect. Values were corrected for the effects of emissivity, including long-wave reflection from the sky.

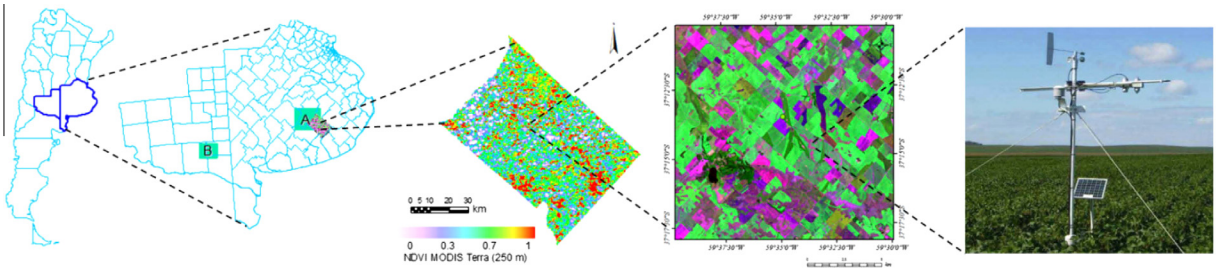

Figure 3 PRA. A and B boxes are the selected areas for the f_c analysis (see Section 6.2), NDVI MODIS (23/02/2010). The central image shows a resized RGB Landsat TM. The right-hand picture is the EBS (37° 14′S, 59° 34′W).

To estimate the joint use with EOS-MODIS and TM sensors, an inversion of the procedure was carried out. The original LST (LST_{HR}) and NDVI ($NDVI_{HR}$) Landsat TM and EOS-MODIS images were aggregated to a resolution of 960 m and 4 km, respectively. Subsequently, the sharpened images were disaggregated and compared with the reference LST (120 m and 1 km, respectively). The agreement between the reference (T_{sref}) and sharpened (T_s^*) temperature images was indicated by the determination coefficient (r^2), root mean square error (RMSE), relative error (RE), mean error (ME) and index of agreement (d). The sharpening models were considered to demonstrate good performance when $r^2 \geqslant 0.8$, $d \geqslant 0.9$, RMSE/σ and RE $\leqslant 0.2$ (Stockle, 2004; Cai et al., 2007). The performance of aggregation was estimated in terms of d (Willmott, 1981) and the RMSE/σ (Kustas et al., 2003).

Different approaches were proposed for the Landsat dataset: *Stepwise resampling* and *resampling by type of coverage*. Stepwise resampling is the downscaling sharpening procedure by steps with multiple spatial resolution sizes (e.g., 960, 720, 240 and 120 m). Resampling by type of coverage considers the process of disaggregation of each class of information from the land use classification. For the EOS-MODIS dataset, sharpening at the *region scale* (*global*) and by *vegetation proportion* approaches were used.

5. Land Surface Temperature (LST) retrieval

The LST for the Landsat TM sensor was calculated from the brightness temperature (T_λ) by applying the Monocanal algorithm proposed by Jimenez-Muñoz and Sobrino (2003):

$$LST = \gamma[\varepsilon^{-1}(\psi_1 L_{\lambda sat} + \psi_2) + \psi_3] + \delta \tag{9}$$

in which

$$\gamma = \{[C_2 L_{\lambda sat}/T_{sat}^2] * [(\lambda_{ef}^4/C_1) * L_{\lambda sat} + \lambda_{ef}^{-1}]\}^{-1} \tag{10}$$

$$\delta = -\gamma L_{\lambda sat} + T_{sat} \tag{11}$$

where $L_{\lambda sat}$ is the radiance retrieved by the TM sensor for channel 6 (W m^{-2} sr^{-1} μm^{-1}), T_{sat} is the brightness temperature (K), λ_{ef} is the effective wavelength (11.457 μm) and C_1 and C_2 are universal constants (1.19104×10^8 W μm^4 m^{-2} sr^{-1} and 1.43877×10^4 μm K, respectively). The values of ψ_1, ψ_2 and ψ_3 were obtained from the atmospheric total water vapour content (W) expressed in gr cm^{-2}. (*University of Wyoming, Department of Atmospheric Science*, http://weather.uwyo.edu).

The emissivity (ε) was estimated using the fraction vegetation cover (f_c) and calibration coefficient proposed by Valor and Caselles (1996).

$$\varepsilon_s = \varepsilon_v f_c + \varepsilon_{su}(1 - f_c) \tag{12}$$

where ε_v is the vegetation emissivity (0.98) and ε_s is the bare soil emissivity (0.96). The cavity effect was not considered, because no internal reflections occur in the dominant vegetation in PRA (natural pastures and agricultural crops) (Kerdiles et al., 1996). The f_c was estimated using NDVI (Carlson and Ripley, 1997).

$$f_c = [(NDVI - NDVI_{MIN})/(NDVI_{MAX} - NDVI_{MIN})]^2 \tag{13}$$

where $NDVI_{MIN}$ represents NDVI values of bare soil and $NDVI_{MAX}$ represents NDVI values of healthy vegetation (total coverage). The NDVI was estimated using the corrected red and near infrared reflectance bands by means of the Dark Object Subtraction technique (DOS), proposed by Schroeder et al. (2006).

$$\rho_{\lambda(\sup)=} \pi(L_{\lambda sat} - L_{\lambda p})/T_{\lambda v} * (E_{\lambda 0} d^{-2} \cos\theta_z T_{\lambda z} + E_{\lambda\downarrow}) \tag{14}$$

where $L_{\lambda sat}$ is the total radiance retrieved by the sensor and $L_{\lambda p}$ is the radiance retrieved by the sensor derived by the interaction between the electromagnetic radiation, gas and atmospheric dust in W m^{-2}sr^{-1}μm^{-1}, $T_{\lambda v}$ is the atmospheric transmissivity from the earth's surface to the sensor, $T_{\lambda z}$ is the atmospheric transmissivity in the solar lighting direction, $E_{\lambda\downarrow}$ is the diffuse irradiance from the atmosphere to the earth's surface (W m^{-2}μm^{-1}) and cos θ_z is the cosine of the solar zenith angle.

For the EOS-MODIS image, this was calculated from the brightness temperature for channels 31 (10.7–11.2 μm) and 32 (11.7–12.2 μm) using the Split Window algorithm developed by Coll et al. (2005). Then, from the temperature difference obtained from the two channels on the same pixel, the LST can be determined using the following equation:

$$LST = T_{31} + [2.41 + 0.432(T_{31} - T_{32})](T_{31} - T_{32}) + 0.359 + \alpha(w)(1 - \varepsilon) + \beta(w)\Delta\varepsilon \tag{15}$$

Here, T_{31} and T_{32} are the brightness temperatures for channels 31 and 32 (K), w is the water vapour content expressed in g cm^{-2}, α and β are parameters that depend on (w), ε is the average emissivity in the 11.2 μm and 12.2 μm intervals ($\varepsilon = (\varepsilon_{31} - \varepsilon_{32})/2$), $\Delta\varepsilon$ is the spectral difference emissivity ($\Delta\varepsilon = \varepsilon_{31} - \varepsilon_{32}$).

6. Results and discussion

6.1. Sharpening at the region scale (global)

To assess the proposed sharpening techniques, an aggregation (upscaling) and disaggregation (downscaling) procedure was applied on EOS-MODIS image (23 February 2010). The procedure takes a Terra aggregated image to 4 km (low resolution) and applies sharpening models until simulated images are obtained with spatial resolution of 1 km. Homogeneity and representative LST samples with spatial independence are required; hence, a random sample of 5% of the pixels was selected and extracted using the semivariogram technique, i.e., an interval of 20 km was used and the random sample extracted.

Fig. 4a shows regression functions between the observed (T_{sref}) and estimated LST data for the EOS-MODIS Terra image (23/02/2010). In all cases, the models performance is similar, the RMSE did not exceed 1 K and the coefficient of determination (r^2) ranged between 0.8–0.9. The T_s^*DL model yielded the smallest RMSE and BIAS (0.7 and 0.0 K, respectively) and the highest aggregation accuracy (RMSE/σ of 0.3).

Fig. 4b shows that the T_s^*FCLS (dashed green) technique indicates slight variability (3.1 K) in comparison with T_{sref} (blue line), whereas the predicted T_s^*DL (black line) is similar to T_{sref} (19.1 K and 19.2 K, respectively). The standard

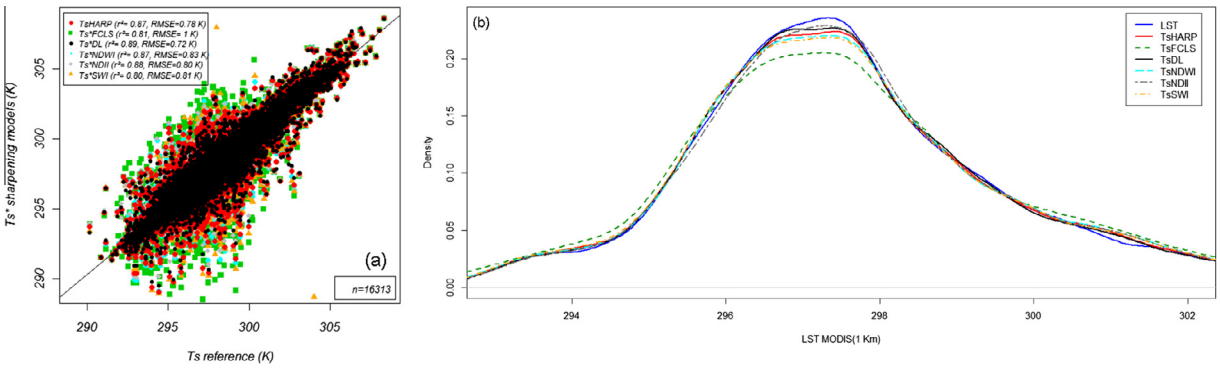

Figure 4 The regression (a) and density (b) of observed and predicted EOS-MODIS LST (23/02/2010).

Table 1 Comparative analysis of different samples.

Models	Semivariogram sample				High f_c sample				Low f_c sample			
	r^2[a]	RMSE[b]	RMSE/σ	d[c]	r^2	RMSE	RMSE/σ	d	r^2	RMSE	RMSE/σ	d
T_sHARP	0.9	0.8	0.4	1.0	0.9	0.4	0.2	1.0	0.9	0.7	0.3	1.0
T_s^*FCLS	0.8	1.1	0.4	0.9	0.9	0.4	0.3	1.0	0.9	0.7	0.3	1.0
T_s^*DL	0.9	0.7	0.3	1.0	0.9	0.4	0.3	1.0	0.9	0.7	0.3	1.0
T_s^*NDWI	1.0	0.8	0.4	1.0	0.9	0.4	0.2	1.0	0.9	0.7	0.3	1.0
T_s^*NDII	0.9	0.8	0.4	1.0	0.9	0.4	0.3	1.0	0.9	0.7	0.3	1.0
T_s^*SWI	0.8	0.8	0.4	1.0	0.9	0.3	0.2	1.0	0.9	0.7	0.3	1.0

N is the observation number, σ is the standard deviation, O_i and E_i are the observed and estimated values and $\overline{O}$ and $\overline{E}$ are the means of the observed and estimated values.

[a] $r^2 = \left[\sum_{i=1}^{N}(E_i-\overline{E})(O_i-\overline{O})\right]^2 / \left[\sum_{i=1}^{N}(E_i-\overline{E})^2\sum_{i=1}^{N}(O_i-\overline{O})^2\right]$.

[b] $RMSE = \left[\sum_{i=1}^{N}(O_i-E_i)^2/N\right]^{1/2}$.

[c] $d = 1-\left[\sum_{i=1}^{N}(O_i-E_i)^2/\sum_{i=1}^{N}(|E_i-\overline{O}|+|O_i-\overline{O}|)^2\right]$.

deviation (σ) and variation coefficient (CV), established as 2.2 K and 0.7%, respectively, show the same values as T_{sref}. The BIAS shows that the models based on the SWIs overestimate the determination and the techniques based on the NDVI-LST relationship underestimate the determination.

6.2. Vegetation proportion

The f_c analysis was realised for two different landscapes of the PRA. The first landscape was located at the centre of the Buenos Aires province (10.120 km^2) (Fig. 3, box A) with high f_c and low water deficit. The second area was located southwest of La Pampa province (4.874 km^2) (Fig. 3, box B), characterised by low f_c and high water deficit.

Table 1 shows the statistical results for the different selected samples (semivariogram, high and low f_c), indicating the high correlation between the samples with high and low f_c. The low f_c samples display an increase in the thermal variability with respect to high f_c, the RMSE <0.3 K for the high f_c samples indicates that the resample techniques are more accurate over regions with high homogeneity in emissivity and soil moisture. The T_s^*SWI model yielded the best disaggregation for high f_c areas (RMSE of 0.3 K and RE of 0.0 K, respectively) with values of r^2 of 0.9, d of 1.0 and RMSE/σ of 0.2 K. Similar results were obtained by the T_s^*DL and T_sHARP models. In terms of the RMSE, the T_s^*DL yielded the best performance considering the semivariogram sample, attaining less than 0.7 K.

6.3. Stepwise resampling

The monitoring of individual fields may become possible if using sharpening EOS-MODIS thermal images to moderate resolution (250 m) and this aspect has been studied by Agam et al. (2007a) using the T_sHARP model. The stepwise procedure shows the utility of the proposed models as applied to EOS-MODIS spatial resolution, simulated with the Landsat TM scene acquired on 23 February 2010. Applying the T_sHARP, T_s^*FCLS, T_s^*DL, T_s^*NDII and T_s^*SWI models to the Landsat image increased the spatial resolution thermal band data from 960 to 120 m. The upper left-hand panel of Fig. 5(A1) shows the 740 m Landsat TM reference thermal image aggregated from 240 m spatial resolution and simulated images (Fig. 5B1–F1) disaggregated by approximations of the EOS-MODIS temperature fields (960 m pixel size). The middle panels (Fig. 5A2–F2) show the 740 m spatial resolution image aggregated to 240 m. The bottom panels (Fig. 5A3–F3) show the 240 m field sharpened to 120 m resolution. Although there are detectable differences between the observed and sharpened fields to 240 m pixel size, in general, the sharpening algorithms recovered much of the detail apparent for the 120 m spatial resolution (Fig. 5A3).

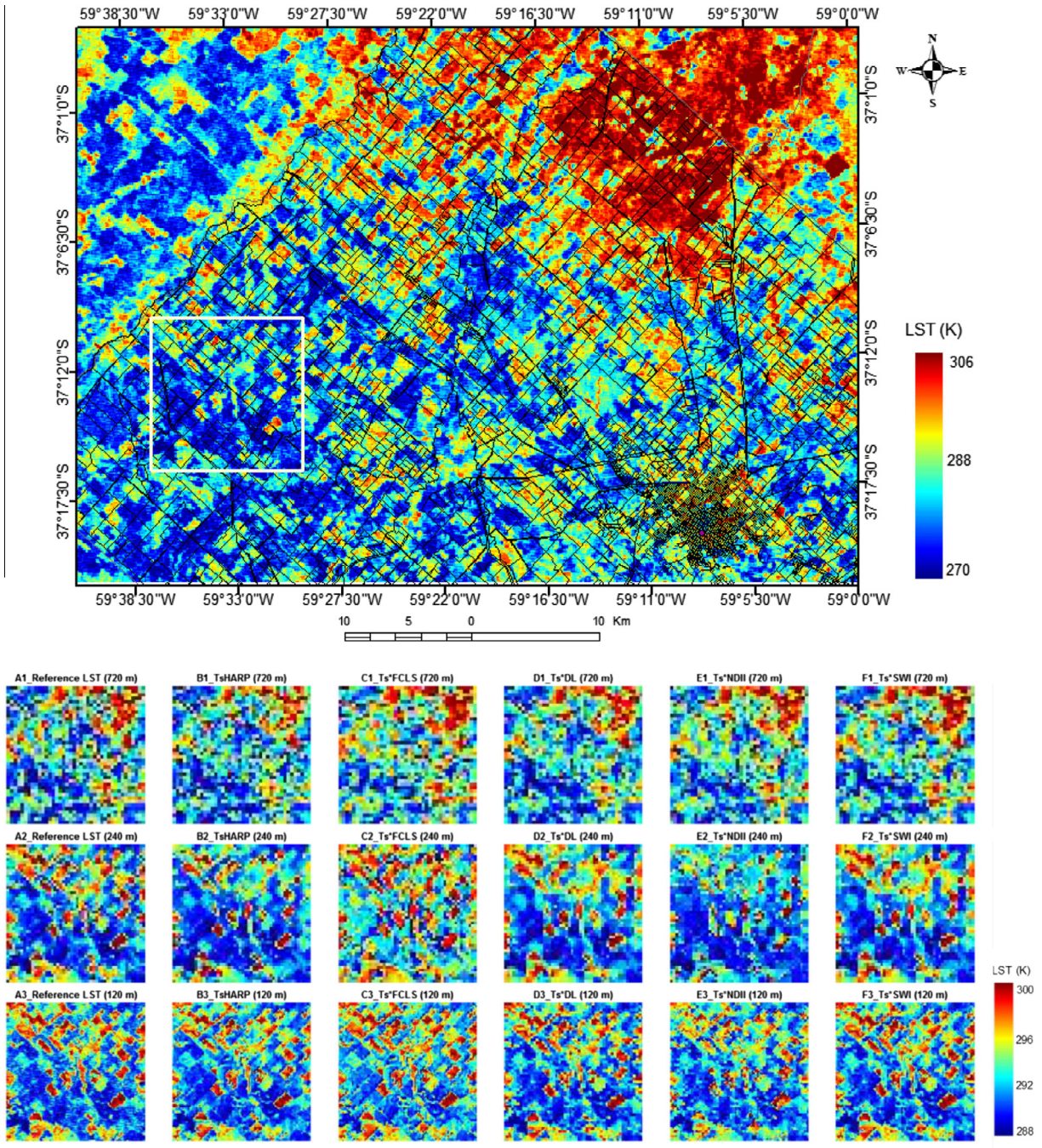

Figure 5 Stepwise performance of the T_sHARP, T_s^*FCLS, T_s^*DL, T_s^*NDII and T_s^*SWI models using the Landsat TM data (23/02/2010). The upper panels (A1–F1 white box in Fig. 5 above) are the aggregated LST of the reference to 720 m pixel size and simulated images from 960 m pixel size (MODIS temperature field). The next panels (A2–F2) are the reference LST and sharpening images to moderate resolution (240 m pixel size) and the lower panels (A3–F3) show the observed temperature field created by the different techniques to 120 m pixel size.

The behaviour of the different techniques for the stepwise analysis denotes a decreasing trend for the r^2 statistic as pixel size decreases, shown by a slight bend at 240 m (Fig. 6a). This trend is observed when large steps in the spatial resolution have been made (e.g., 720 to 240 m). Fig. 6b shows the statistical errors for different resolutions; the higher RMSEs were observed between 720 and 240 m spatial resolutions with a stepwise increasing trend. Highest accuracy was reached by the T_s^*FCLS and T_s^*SWI techniques at 720 m pixel size with an RMSE of 0.7 K without slant. However, the trend remained invariant for the T_s^*DL model (Fig. 6b, black bar) through the stepwise procedure and it was slightly lower than that found by Agam et al. (2007a) and Kustas et al. (2003). Homogeneous interquartile ranges were observed for different sharpening techniques; the best performances were reached by the T_s^*DL and T_s^*SWI models, which were 19.1 and 19.1 K, respectively.

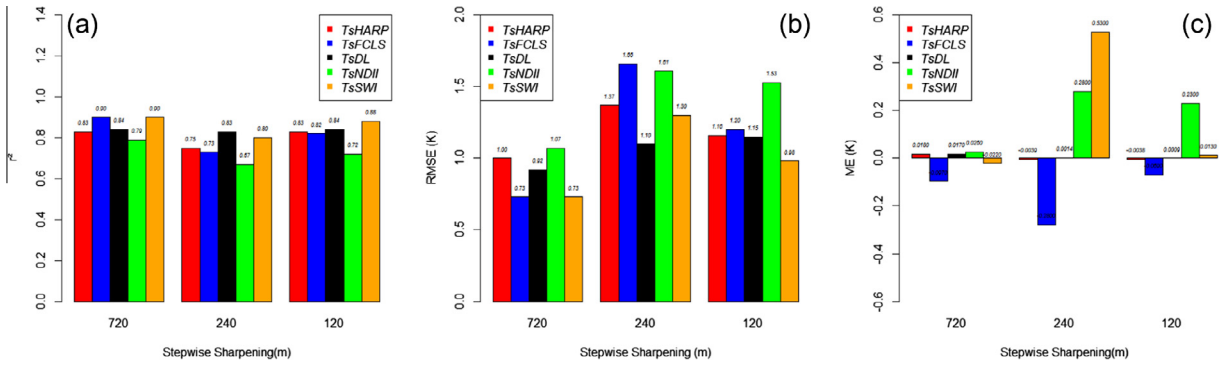

Figure 6 Comparative analysis of different sharpening procedures to 720, 240 and 120 m pixel sizes. (a) r^2, (b) RMSE and (c) ME.

Table 2 Comparative statistics between the observed.

Statistics (K)	LST ref	T_sHARP	T_s^*FCLS	T_s^*DL	T_s^*NDII	T_s^*SWI
Min	274.9	276.4	275.7	275.3	273.8	275.6
1st Q	292.2	292.1	292.0	292.2	292.4	292.1
Median	294.5	294.4	294.4	294.4	294.6	294.4
Average	294.3	294.3	294.3	294.3	294.5	294.3
3rd Q	296.2	296.3	296.3	296.2	296.4	296.2
Max	306.4	306.3	305.8	306.4	311.1	305.8
Range	31.4	29.9	30.0	30.1	37.3	30.1
σ	2.7	2.9	2.9	2.8	2.9	2.8
CV (%)	0.9	1.0	1.0	1.0	1.0	1.0
Skewness	0.0	0.0	0.0	0.0	0.0	0.0
Curtosis	0.2	0.0	0.0	0.2	0.4	0.0
RMSE		1.0	1.0	0.6	1.0	0.8
RE[a]		0.0	0.0	0.0	0.0	0.0
ME[b]		0.0	0.0	0.0	0.1	0.0
d		1.0	1.0	1.0	1.0	1.0
RSME/σ		0.3	0.4	0.2	0.4	0.3

[a] $RE = RMSE/\bar{O}$.
[b] $ME = \sum_{i=1}^{N}(O_i - E_i)/N$.

The thermal variability for the T_sHARP and T_s^*FCLS models to 120 m pixel size were incremented, which indicates that the variability was limited to extreme values because the moisture conditions were strongly variable. Fig. 6c indicates that the T_sHARP and T_s^*DL techniques did not overestimate or underestimate the LST prediction (without BIAS). The remaining models indicate high BIAS where there are significant scale breaks.

Jeganathan et al. (2011) studied the cause of the variations in the upscaled ASTER–LST at 1 km pixel size with the MODIS–LST from the perspective of stepwise downscaling analysis, aggregation methods and retrieval parameters of interest. Their study observed that, just as here, the statistical errors and function adjustments (slope) at different resolutions increases as the resolution decreases due to the incremented spatial heterogeneity. However, Jeganathan et al. (2011) indicate that the value of r^2 decreases with a decrease in pixel size, which is explained by the reduction of variability in the LST and NDVI by the aggregation; in the present study, this effect occurred only with long steps (e.g., 720–240 m) (Fig. 6a).

In general, the stepwise analysis indicates that the performance of the different models was better than that found by Agam et al. (2007a) and Kustas et al. (2003), which could be due to the limited accuracy of the retrieved LST and geometric correction between images (EOS-MODIS vs. Landsat). Liu et al. (2006) observed that the limited accuracy of the retrieved LST was the largest source of error in the sharpening procedure. Also, according to Jeganathan et al. (2011), an inadequate geometric correction (RMSE of less than 1 pixel) and non-multiple pixel size (e.g., 250–120 m) could introduce uncertainty and inaccuracy to the sharpened image.

The reference LST (120 m) was aggregated to 30 m by applying the different sharpening techniques with the aim of assessing the performance to fine spatial resolution. Using the semivariogram technique, random samples of 4% of overall image were selected (57.481 pixels) to obtain a statistically representative number of pixels. Spatial independence was reached at 40 and 60 pixels, taking into account the spatial range of 100 pixels and considering a mean distance threshold of 50 pixels (1500 m).

Table 2 shows the statistics for the observed and predicted LST; the range and mean show similar thermal variability with respect to the reference LST. Otherwise, a wide disparity was found for the T_s^*NDII model with a value of 37.3 K. A high degree of aggregation is indicated for the T_s^*DL and T_s^*SWI models with d less than 1.0, RMSE/σ of 0.3 and RMSE of 0.6–0.8 K, respectively.

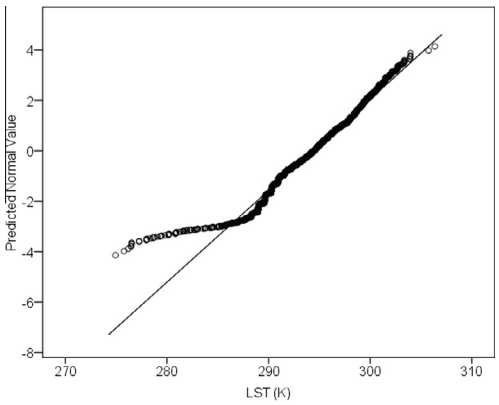

Figure 7 Q–Q plot of observed vs. predicted LST values.

The quantile–quantile (Q–Q) plot in Fig. 7 shows high correlation between the thermal reference data to 30 m with respect to the normal line from the mean to the highest LST values. Hence, the smallest LST values are separate with respect to the normal line, indicating pixels with high thermal variability due to the different proportions of bare soil and vegetation. This trend was observed for all sharpening techniques.

6.4. Resampling by type of coverage

The model performances were assessed for different land cover types classified on the Landsat TM image (23 February 2010). By applying the unsupervised ISODATA algorithm, five classes of interest were identified (1st and 2nd soybean, sunflower, corn and bare soil) with 98% accuracy (Kappa coefficient of 0.9). Fig. 8 shows the model behaviours for different types of cover evaluated by 1000-pixel-sized samples.

Note that the soybean classes demonstrate a trend to decrease the accuracy (worst adjustment), which is because the LST representation results in greater complexity for vegetation cover with variable soil moisture (Fig. 8a). The T_sHARP (red bar) and T_s^*NDII (green bar) models yielded poor performance, achieving RMSEs of 1.2 and 3.0 K (Fig. 8b). These errors might be related closely to the stage of the vegetation senescense. Moreover, the T_s^*DL technique (black bar) showed the best predictions: 0.7 K RMSE and 0.0 RE, which remained invariant for the different classes (BIAS of 0.0 K, Fig. 8c). Also, the best data aggregation was achieved for corn and bare soil classes using the T_s^*DL model with 0.3 and 0.4 RMSE/σ, respectively. Similar values are indicated for the T_s^*SWI model (orange bar).

6.5. Validation

The validation was realised considering good performance of the T_s^*DL technique for different resolutions and surface conditions. The validation accounted for the *in situ* measurements observed over the soybean and wheat (transect) fields. The comparison between the pixel results and IRR-1505 sensor at the EBS shows that the LST was 294.8 K, that yielded by the EOS-MODIS resampling was 293.9 K and that from the Landsat resampling was 292.9 K.

The validation of the thermal resampled data (10/11/2006 Landsat TM dataset) was performed on 38 resampled measurements from a transect over a test site with wheat crop (Fig. 9a). Local-scale values show a variability that can be considered significant but this assumption is not considered on the field scale. Therefore, the resampling technique is optimal for a considered scale (Fig. 9b, orange solid line and dashed green line). The mean value obtained with the T_s^*DL model was 291.5 ± 0.9 K and that from the T_sHARP model was 292.3 ± 0.5 K based on the Landsat image, whereas for the transect it was 291.4 ± 1.1 K. Moreover, the values obtained from the EOS-MODIS data have a difference of 3.0 K compared with those measured *in situ*.

Fig. 10 (a and b) shows the LST Landsat image and the estimated Ts^*DL MODIS products to 30 m spatial resolution, respectively; the LST sub-pixel estimation results have hidden the LST changes. As shown in Fig. 10b, the spatial distribution of high temperatures over areas of bare soil (B) is overestimated. Moreover, the spatial distribution of low temperatures (A) over areas of wheat coverage is underestimated compared with the real situation.

The results on the disaggregation of the EOS-MODIS LST data from a spatial resolution of 1000–30 m showed that the sharpening was less accurate than with the Landsat TM for a similar resolution difference (960–30 m). However, this may be due to the sensor used to generate the data (EOS-MODIS vs. Landsat TM) and the fact that the pixel of the thermal MODIS image is the mean value of the different land cover types contained in the scene. Hence, we support the idea that the disaggregation of the EOS-MODIS LST data to 250 m is adequate for representing the heterogeneity of the PRA, mainly because the size is bigger than 50 ha.

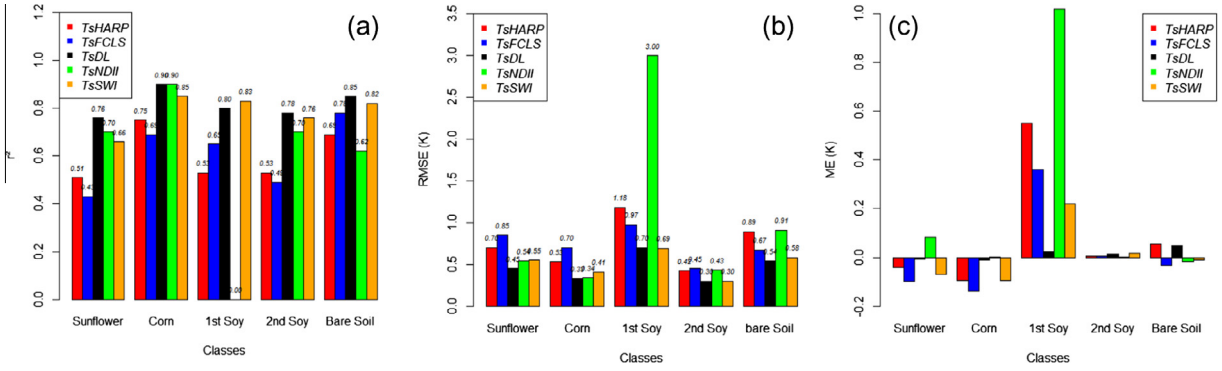

Figure 8 Comparative analysis of different land covers. (a) r^2, (b) RMSE and (c) ME.

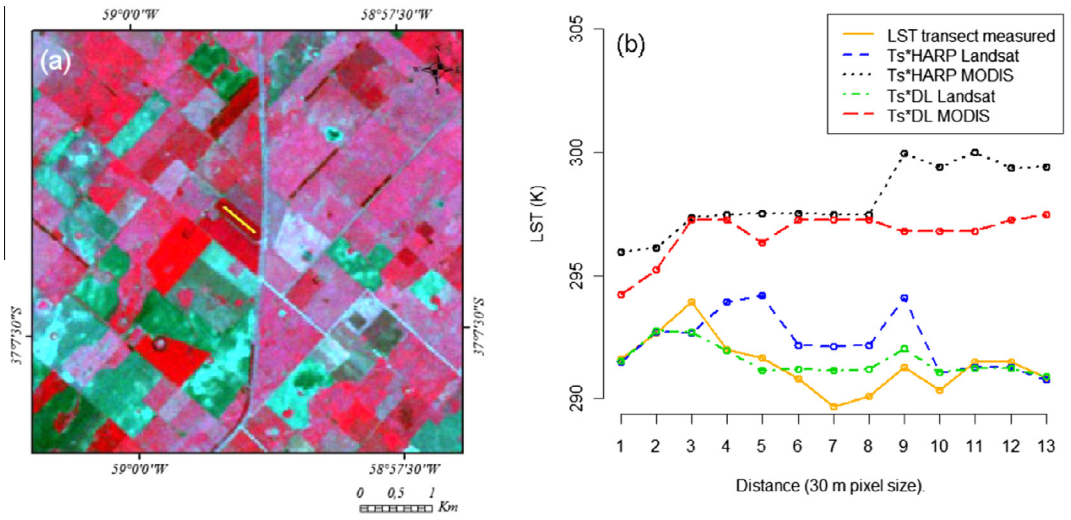

Figure 9 (a) Landsat TM (10/11/2006) sample in RGB composition and validation transect (yellow line). b) LST (K) transect measured and thermal data yielded by the T_sHARP and T_s^*DL models.

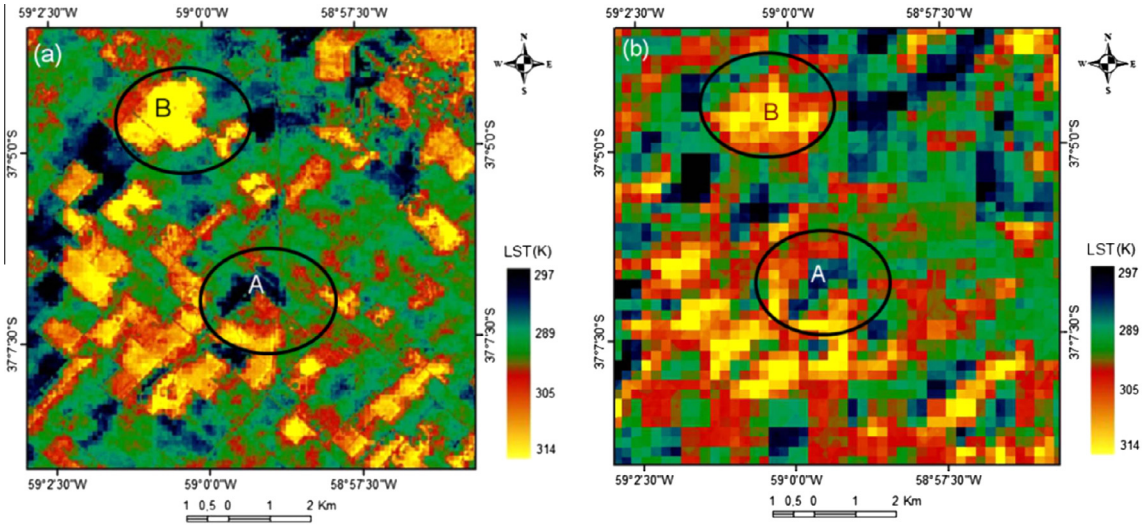

Figure 10 (a) LST Landsat image (30 m) with wet (A) and dry (B) areas. (b) The estimated T_s^*DL MODIS (30 m) image with wet (A) and dry (B) areas.

7. Summary and conclusion

The need for high spatial–temporal resolution thermal data has led to further modification of the T_sHARP procedure. In this study, six different sharpening procedures with the same theoretical basis, using and combining thermal/visible spatial information of EOS-MODIS and TM sensors, were proposed and evaluated in the PRA. The performance of the procedures was found to depend on the dry and wet edge definition in the LST–NDVI relationship. It was observed that the results improved when using the quadratic dry edge fitting, mainly because that function finds the maximum LST value where NDVI values are low (minimal evapotranspiration); thus, acquiring more physical sense.

The sensitivity in the estimation of the sub-pixel LST depends on the proportion of soil and vegetation in each resampled pixel. In EOS-MODIS, for areas with little variability of surface emissivity, the errors were of the order of 0.3 K for high f_c areas. However, in areas with low f_c and low soil moisture, the errors increased to 0.7 K. The T_s^*DL model showed good results for corn and wet bare soil with a correlation greater than 85% and low RMSE (from 0.3 to 0.5 K) for Landsat images.

The T_s^*DL model was the most accurate and stable sharpening method from low to high spatial resolution images. Thus, it would be useful for representing spatial patterns of LST with reasonable accuracy within each pixel of Terra MODIS and Landsat TM images of the PRA.

Although the T_s^*DL algorithm has been proven more accurate than T_sHARP in this study, both thermal image sharpening techniques are still unable to consider the sub-pixel soil moisture variation. Hence, information about the sub-pixel variability for moisture was introduced to the sharpening techniques by water stress indices such as *NDWI*, *NDII* and *SWI*. However, with the exception of the T_s^*SWI model, the techniques based on water stress index were less accurate than

algorithms based on the LST–NDVI relationship only. Future work may involve information about the sub-pixel variability for moisture to improve the sharpening capacity.

Acknowledgements

This article was financed by the National Commission of Space Activities (CONAE), Commission of Scientific Research of Buenos Aires Province (CIC), Ministry of Science, Technology and Innovation Production (MINCyT).

References

Agam, M.C., Kustas, W.P., Anderson, M., Li, F., Neale, C.M.U., 2007a. A vegetation index based technique for spatial sharpening of thermal imagery. Remote Sens. Environ. 107, 545–558.

Agam, N., Kustas, W.P., Anderson, M.C., Li, F., Colaizzi, P.D., 2007b. Utility of thermal sharpening over Texas high plains irrigated agricultural fields. J. Geophys. Res. 112, D19110. http://dx.doi.org/10.1029/2007JD08407.

Cai, J., Liu, Y., Pereira, L.S., 2007. Estimating reference evapotranspiration with the FAO Pennam–Monteith equation using daily weather forecast massages. Agric. For. Mereorology 145, 22–35.

Carmona, F., Rivas, R., Caselles, V., 2012. Estimate of the alpha parameter in an oat crop under rain-fed conditions. Hydrol. Process.. http://dx.doi.org/10.1002/hyp. 9415.

Carlson, T.N., Ripley, D.A., 1997. On the relation between NDVI, fractional vegetation cover, and leaf area index. Remote Sens. Environ. 62, 241–252.

Chen, L., Yan, G., Ren, H., Li, A., 2010. A modified vegetation index based algorithm for thermal imagery sharpening. IGARRS-IEEE, 978-1-4244-9566-5/10.

Chen, Y., Zhan, W., Quan, J., Zhou, J., Zhu, X., Sun, H., 2014. Disaggregation of remotely sensed land surface temperature: a generalized paradigm. IEEE Trans. Geosci. Remote Sens..

Coll, C., Caselles, V., Galve, J.M., Valor, E., Niclós, Raquel., Sanchez, J., Rivas, R., 2005. Ground measurements for the validation of land surface temperatures derived from AATSR and MODIS data. Remote Sens. Environ. 97, 288–300.

Gao, B.C., 1996. NDWI a normalized difference water index for remote sensing of vegetation liquid water from space. Remote Sens. Environ. 58, 257–266.

Hardisky, M.A., Klemas, V., Smart, R.M., 1983. The influences of soil salinity, growth form, and leaf moisture on the spectral reflectance of Spartina alterniflora canopies. J. Photogramm. Remote Sens. 49, 77–83.

Holzman, M.E., Rivas, R., Piccolo, M.C., 2014. Estimating soil moisture and the relationship with crop yield using surface temperature and vegetation index. Int. J. Appl. Earth Obs. Geoinf. 28, 181–192.

Jeganathan, C., Hammb, N.A.S., Mukherjeec, S., Atkinsona, P.M., Rajud, P.L.M., Dadhwale, V.K., 2011. Evaluating a thermal image sharpening model over a mixed agricultural landscape in India. Int. J. Appl. Earth Obs. Geoinf. 13, 178–191.

Jimenez-Muñoz, J., Sobrino, J., 2003. A generalized single channel method for retrieving land surface temperature from remote rensing data. J. Geophys. Res. vol.118.

Kerdiles, H., Grondona, M., Rodriguez, R., Seguin, B., 1996. Frost mapping using NOAA AVHRR data in the Pampean region, Argentina. Agric. For. Meteorol. 79, 157–182.

Kim, G., Barrows, A.P., 2002. Downscaling of remotely sensed soil moisture with a modified fractal interpolation method using contraction mapping and ancillary data. *Remote Sens. Environ.* 83, 400–413.

Kustas, W.P., Li, F., Jackson, T.J., Prueger, J.H., MacPherson, J.I., Wolde, M., 2004. Effect of remote sensing pixel resolution on modeled energy flux variability of croplands in Iowa. Remote Sens. Environ. 92, 535–547.

Kustas, W.P., Norman, J.M., Anderson, M.C., French, A.N., 2003. Estimating subpixel surface temperatures and energy fluxes form the vegetation index-radiometric temperature relationship. Remote Sens. Environ. 85, 429–440.

Li, F., Kustas, W.P., Anderson, M.C., Prueger, J.H., Scott, R.L., 2008. Effect of remote sensing pixel resolution on interpreting tower-based flux observations. Remote Sens. Environ. 112, 337–349.

Liu, Y., Hiyama, T., Yamaguchí, Y., 2006. Scaling of land surface temperature using satellite data: a case examination on ASTER and MODIS products over a heterogeneous terrain area. Remote Sens. Environ. 105, 115–128.

Liu, D., Pu, R., 2008. Downscaling thermal infrared radiance for subpixel land surface temperature retrieval. Sensors 8, 2695–2706.

Mallick, K., Bhattacharya, B.K., Patel, N.K., 2009. Estimating volumetric surface moisture content for cropped soils using a soil wetness index based on surface temperature and NDVI. Agric. For. Meteorol. 149, 1327–1342.

Merlin, O., Al Bitar, A., Walker, J.P., Kerr, Y., 2009. A sequential model for disaggregating near-surface soil moisture observations using multi-resolution thermal sensors. Remote Sens. Environ. 113, 2275–2284.

Merlin, O., Walker, J.P., Chehbouni, A., Kerr, Y., 2008. Towards deterministic down-scaling of SMOS soil moisture using MODIS derived soil evaporative efficiency. Remote Sens. Environ. 112, 3935–3946.

Rodriguez-Galiano, V., Pardo-Izquierdo, E., Sanchez Castillo, M., Chica-Olmo, M., Chica-Rivas, M., 2012. Downscaling Landsat 7 ETM + thermal imagery using land surface temperature and NDVI images. Int. J. Appl. Earth Obs. Geoinf. 18, 515–527.

Rouse, J. W., Haas, R. H., Schell, J. A., Deering, D. W., and Harlan, J. C., 1974. Monitoring the vernal advancement and retrogradation (greenwavee effect) of natural vegetation. NASA/GSFC Type III Final Report, Greenbelt, Maryland..

Sandholt, I., Rasmussen, K., Andersen, J., 2002. A simple interpretation of the surface temperature/vegetation index space for assessment of surface moisture status. Remote Sens. Environ. 79, 213–224.

Schroeder, T.A., Cohen, W.B., Song, C., Canty, M.J., Yang, Z., 2006. Radiometric correction of multi-temporal Landsat data for characterization of early successional forest patterns in western Oregon. Remote Sens. Environ. 103, 16–26.

Stockle, C.K., 2004. Evaluation of estimated weather data for calculating Panman–Monteith reference evapotranspiration. Irrig. Sci. 23, 39–46.

Sun, D., Kufatos, M., 2007. Note on the NDVI-LST relationship and the use of temperature-related. Geophys. Res. Lett. 34, L24406. http://dx.doi.org/10.1029/2007GL031485.

Valor, E., Caselles, V., 1996. Mapping land surface emissivity from NDVI: application to European, African and South American areas. Remote Sens. Environ. 57, 167–184.

Willmott, C.J., 1981. On the variation models. Phys. Geogr. 2, 184–194.

Yang, G., Pu, R., Zhao, C., Huang, W., Wang, J., 2011. Estimation of subpixel land surface temperature using an endmember index based technique: A case examination on ASTER and MODIS temperature products over a heterogeneous area. Remote Sens. Environ. 115, 1202–1219.

Zurita-Milla, R., Kaiser, G., Clevers, J.G.P.W., Schneder, W., Schaepman, M.E., 2009. Downscaling time series of MERIS full resolution data to monitor vegetation seasonal dynamics. Remote Sens. Environ. 113, 1874–1885.